

Magnetic field controlled charge density wave coupling in underdoped $\text{YBa}_2\text{Cu}_3\text{O}_{6+x}$

J. Chang,¹ E. Blackburn,² O. Ivashko,¹ A. T. Holmes,³ N. B. Christensen,⁴ M. Hückler,⁵ Ruixing Liang,^{6,7} D. A. Bonn,^{6,7} W. N. Hardy,^{6,7} U. Rütt,⁸ M. v. Zimmermann,⁸ E. M. Forgan,² and S. M. Hayden⁹

¹*Physik-Institut, Universität Zürich, Winterthurerstrasse 190, CH-8057 Zürich, Switzerland*

²*School of Physics and Astronomy, University of Birmingham, Birmingham B15 2TT, United Kingdom.*

³*European Spallation Source ERIC, Box 176, SE-221 00 Lund, Sweden*

⁴*Department of Physics, Technical University of Denmark, DK-2800 Kongens Lyngby, Denmark.*

⁵*Condensed Matter Physics & Materials Science Dept., Brookhaven National Lab., Upton, NY 11973, USA.*

⁶*Department of Physics & Astronomy, University of British Columbia, Vancouver, Canada.*

⁷*Canadian Institute for Advanced Research, Toronto, Canada.*

⁸*Deutsches Elektronen-Synchrotron DESY, 22603 Hamburg, Germany.*

⁹*H. H. Wills Physics Laboratory, University of Bristol, Bristol, BS8 1TL, United Kingdom.*

(Dated: March 6, 2022)

The application of large magnetic fields ($B \sim B_{c2}$) to layered cuprates suppresses their high temperature superconducting behaviour and reveals competing ground states^{1,2}. In the widely-studied material $\text{YBa}_2\text{Cu}_3\text{O}_{6+x}$ (YBCO), underdoped ($p \sim 1/8$) samples show signatures of field-induced electronic^{3,4} and structural^{5,6} changes at low temperatures. However, the microscopic nature of the field-induced reconstruction and the high-field state are unclear. Here we report an x-ray study of the high-field charge density wave (CDW) in YBCO, for doping, $0.1 \lesssim p \lesssim 0.13$. For $p \sim 0.123$, we find that a field ($B \sim 10$ T) induces new CDW correlations along the CuO chain (b) direction only, leading to a 3-D ordered state along this direction⁶ at $B \sim 15$ T. The CDW signal along the a -direction is also enhanced by field, but does not develop a new pattern of correlations. We find that field modifies the coupling between the CuO_2 bilayers in the YBCO structure, and causes the sudden appearance of 3D CDW order. The mirror symmetry of individual bilayers is broken by the CDW at low and high fields, allowing recently suggested^{7,8} Fermi surface reconstruction.

Charge density wave (CDW) correlations⁹, that is, periodic modulations of the electron charge density accompanied by a periodic distortion of the atomic lattice, are now believed to be a universal property of underdoped HTC superconductors^{3,10–16}. CDW correlations appear at temperatures well above the superconducting T_c . Cooling through T_c suppresses the CDW and leads to a state where the superconducting and CDW order parameters are intertwined and competing.

The application of magnetic fields $B \sim B_{c2}$ suppresses superconductivity. For underdoped YBCO, fields $B \approx 10 - 20$ T cause changes in the CDW order which can be seen by x-ray measurements^{6,12} and also give changes in ultra-sound⁵ and NMR³ signals. At larger fields, $B \gtrsim 25$ T a normal state is observed with a Fermi surface having electron pockets^{17,18} and coherent trans-

port along the c -axis¹⁹. Here we report hard x-ray scattering measurements of the evolution of the CDW correlations with magnetic fields up to 16.9 T for several doping levels. We investigated CDW propagation vectors along the crystallographic a - and b -directions, allowing us to extend recent pulsed-field measurements⁶ and identify the new field-induced anisotropies in the CDW.

The CDW correlations in the cuprates have propagation vectors with the in-plane components parallel to the Cu-O bonds and periodicities of $3 - 4a$ depending on the system^{11,12,20,21}. YBCO shows a superposition of modulations localised near the CuO_2 bilayers, with basal plane components of their propagation vectors along both a and b : $\mathbf{q}_a = (\delta_a, 0, 0)$ and $\mathbf{q}_b = (0, \delta_b, 0)$ with correlation lengths up to $\xi_a \approx 70\text{\AA} \approx 20a$. Both \mathbf{q}_a and \mathbf{q}_b CDWs have ionic displacements perpendicular to the CuO_2 bilayers combined with displacements parallel to these planes, which are $\pi/2$ out of phase²². These give rise to scattering along lines in reciprocal space given by $\mathbf{Q}_{\text{CDW}} = n\mathbf{a}^* + m\mathbf{b}^* + \ell\mathbf{c}^* \pm \mathbf{q}_{a,b}$, where n and m are integers. The distribution of the scattered intensity along ℓ depends on the relative phase of the CDW modulations in the bilayers stacked along the c direction. In zero magnetic field, there is weak correlation of phases in neighbouring bilayers and we observe scattered intensity spread out along the \mathbf{c}^* direction, peaked at $\ell \approx 0.5$. This is illustrated by our x-ray measurements on $\text{YBa}_2\text{Cu}_3\text{O}_{6.67}$ ($p = 0.123$, $T_c = 67$ K, ortho-VIII CuO -chain ordering), shown in Fig. 1a,f. Note that the strong scattering around $\mathbf{Q} \sim (13/8, 0, 0)$ in Fig. 1a,b is due the CuO -chain ordering, which does not change with field, and can be subtracted, as in Fig. 1c,d. By taking cuts through the data, we obtain the intensity of the CDW scattering versus ℓ for the \mathbf{q}_a and \mathbf{q}_b positions (Fig. 1e,j).

Fig. 1 shows that the effect of applying a magnetic field is very different for two components (\mathbf{q}_a and \mathbf{q}_b) of the CDW. For the \mathbf{q}_a component of the correlations (Fig. 1b), the rod of scattering becomes stronger with no discernible change in the ℓ width or position of the maximum *i.e.* the correlations simply become stronger.

In contrast, for the \mathbf{q}_b correlations (Fig. 1i) we see two qualitative changes. First, at $B \approx 10$ T, the rod of diffuse scattering becomes broader and its peak position begins to move to larger ℓ . Second, at $B \approx 15$ T, a new peak (shaded pink and first reported in Ref. 6) appears centred on $\ell = 1$, but only for the \mathbf{q}_b component. The new peak indicates that the sample has regions where the CDW modulation is in phase in neighbouring bilayers and is coherent in three spatial directions. These regions would have a typical length along the c -axis of $\xi_c \approx 47$ Å.

We measured the intensity of the new 3D CDW order in 14 different Brillouin zones. These data (see Supplementary Information) are consistent with the high-field CDW structure of an individual bilayer being unchanged from that determined at zero field²². Both low- and high-field structures break the mirror symmetry of a bilayer, but in the high field structure (see Fig. 3a,d), the atomic displacements in adjacent bilayers are in phase. Thus, the high-field order has $\mathbf{q}_b = (0, \delta_b, 0)$; however, its structure yields zero CDW intensity for $\ell = 0$ and nonzero for $\ell = 1$ positions, as we observe (see Supplementary Information). The relationship between the CDW structures at low and high field is to be expected, since the coupling between the two CuO_2 planes in a bilayer will be stronger than coupling with another bilayer. For the other basal plane direction, no CDW signal was found at $\mathbf{q}_a = (\delta_a, 0, 0)$ or $(\delta_a, 0, 1)$ for $B \leq 16.9$ T (see Fig. 2c).

The ℓ -dependent profiles in Fig. 1e,j contain information about the correlation between the phases of the CDW modulation in the bilayers stacked along the c -axis. For $B = 0$, the broad $\ell \approx 0.5$ peaks in Fig. 1e,j for \mathbf{q}_a and \mathbf{q}_b indicate that the CDW phase is weakly anti-correlated between neighbouring bilayers. On increasing the field above $B \approx 10$ T, the ℓ -profile of the \mathbf{q}_b correlations evolves. The onset of this evolution can be seen as an increase in the intensity of the scattering at $(0, 4 - \delta_b, 1)$ (Fig. 4c), signalling the introduction of new c -axis correlations. This change is accompanied by a growth of correlations along the b -axis, as shown by the increase in the correlation length $\xi_{b,\ell=1}$ measured by the peak width of scans parallel to \mathbf{b}^* through the $(0, 4 - \delta_b, 1)$ position (see Fig. 4e). We describe this state as “3D CDW precursor correlations”. The onset temperature $T \approx 65$ K of the precursor correlations at high field ($B = 16.5$ T) may be determined from the increase in $\xi_{b,\ell=1}$ and the scattering intensity at the $(0, 4 - \delta_b, 1)$ position (Fig. 4c,e). This allows us to designate a region of the $B - T$ phase diagram (see Fig. 5).

At higher fields, $B \gtrsim 15$ T, a peak (shaded pink in Fig. 1j) develops abruptly in the ℓ -profile at $\ell = 1$. The abrupt onset of the peak signals a rapid growth of the c -axis correlation length ξ_c (Fig. 4d,e). The growth of correlations in one spatial direction followed by growth in a second direction is typical of systems with anisotropic coupling. Another CDW system which shows this behaviour²³ is NbSe_3 . Large correlated regions develop first in planes where the order parameter is most strongly coupled. These act to amplify the coupling in

the remaining direction. In case of $\text{YBCO}_{6.67}$, the in-plane correlation length continues to grow down to low temperatures with $\xi_{b,\ell=1} = 80b = 310$ Å (at ~ 10 K and 16.5 T). The c -axis correlation length, however, saturates with $\xi_{c,\ell=1} = 47$ Å at $T \approx 30$ K suggesting disorder limited correlations. All these changes together signal the transition to a new phase (see Fig. 5 pink region) which we label “3D CDW order” identified with a phase transition also seen in ultrasound⁵ and thermal Hall effect⁴ measurements. At the lowest temperatures, $T \lesssim 25$ K, we observe (Fig. 4a) a suppression of the 3D CDW peak intensity signalling a competition between the superconducting and 3D CDW order parameters.

Previous x-ray^{11,12} and NMR²⁴ on $\text{YBCO}_{6.67}$ have shown that the weak anti-phase ($\ell = 1/2$) CDW correlations appear at $T \approx 150$ K. Further NMR anomalies in the form of line splittings^{3,25} are observed at $T \approx 65$ K for $B = 28.5$ T and at $B \approx 10$ T for $T = 2$ K. These anomalies which are displayed on Fig. 5 appear to coincide with the onset of the 3D precursor correlations reported here. The fact that NMR sees similar transitions shows that the 3D CDW precursor correlations we observe are static on timescales $\tau \gtrsim 0.1$ ms. Correlations that are static²⁴ and short ranged are necessarily controlled by pinning with quenched disorder playing a role.

We also studied other dopings of $\text{YBa}_2\text{Cu}_3\text{O}_{6+x}$. For $\text{YBCO}_{6.60}$ ($p = 0.11$) with ortho-II oxygen chain structure, a very similar onset field (Fig. 5) and c -axis correlation length ξ_c were found. In $\text{YBCO}_{6.51}$ and $\text{YBCO}_{6.75}$, no 3D order was observed for $B \leq 16.9$ T (Fig. 2a). However, we do observe the precursor movement of the CDW scattering to higher ℓ implying that this structure is likely to appear at higher fields. Thus, the 3D order is most easily stabilized for doping around $p = 0.11 - 0.12$ (see Fig. 5b).

A simple statistical approach based on a Markov chain (See Methods) can be used to model possible CDW stacking sequences along the c -axis and compute the scattering profile as a function of ℓ . A good description of our data is obtained if we assume that the CDW phase difference between neighbouring bilayers is 0 or π (see Supplementary Information). The parameters in our model are the nearest- and next-nearest-neighbour couplings β and γ , where positive values favour the same phase. At $B = 0$, the model shows that the broad $\ell \approx 0.5$ peaks in Fig. 1e,j are due to weakly anti-correlated bilayers (see Fig. 3b,e). The field-evolution of the ℓ -dependent profiles for \mathbf{q}_b (Fig. 1j), including the formation of the $\ell = 1$ peak, may be modelled by as a continuous variation of β and γ from anti-phase coupling at low field to same-phase coupling at high field (see Fig. 3e). The sign of β changes near the onset of the 3D order at $B \approx 15$ T. Thus we find that a c -axis magnetic field can control the coupling between the CDWs in neighbouring bilayers. The field-control of the coupling most likely arises through the suppression of superconductivity by field. Magnetic field strengthens the correlations along the a -axis (Fig. 1e), however, it does not increase correlation lengths. Possible

explanations for this difference in behaviour include the influence of the CuO chains promoting the b -axis modulations or the chains pinning the a -axis CDW modulations.

We conclude that the appearance of 3D CDW order corresponds to the onset of new c -axis electronic coherence and hence electronic reconstruction. This is supported by thermal Hall conductivity measurements⁴ which demonstrate Fermi-surface reconstruction at the same field (see Fig. 5a). At highest fields investigated, $B = 16.9$ T, the structure of the CDW within individual bilayers involves the same breaking of mirror symmetry observed at zero field²² which has been posited to lead to Fermi surface reconstruction^{7,8}.

Methods

Experimental details Our experiments used 98.5 keV hard X-ray synchrotron radiation from the PETRA III storage ring at DESY, Hamburg, Germany. A 17 T horizontal cryomagnet was installed at the P07 beamline, providing essentially identical scattering conditions to those described in Ref. 12. Access to the $(h, 0, \ell)$ and $(0, k, \ell)$ scattering planes was obtained by aligning either the a - c axes or the b - c axes horizontally, with the c -axis approximately along the magnetic-field and beam direction. The samples were glued to a pure aluminium plate on which was mounted a Cernox[®] thermometer for measurement and control of temperature. With the high intensities of PETRA III, a small amount of beam heating of the sample was observed. By observing the effect of changes in beam heating (controlled by known attenuation) on the measured temperature of the 3-D phase transition we determined the effect of the beam on the sample temperature near 40 K. The sample heating at other temperatures was determined using the Cernox thermometer and a model of the heat flow from the sample to the aluminium plate. We estimate that there is an absolute uncertainty in our temperature determination of ± 2 K. The relative temperature uncertainty is smaller than this.

y in YBCO	Oxygen ordering	Doping level p	T_c (K)	B_c (T)	ξ_b (b)	ξ_c (c)
6.51	o-II	0.096	59	> 16.9	-	-
6.60	o-II	0.11	61.8	15.3 ± 0.35	48	4.5
6.67	o-VIII	0.123	67	14.5 ± 0.5	80	4
6.75	o-III	0.132	74	> 16.9	-	-

TABLE I: YBCO samples investigated in this study. The correlation length ξ_b and ξ_c of the $(0, \delta_b, 0)$ CDW order at the highest measured fields and lowest temperature are given in units of the lattice parameters $b \sim 3.87$ and $c = 11.7$ Å.

Four YBCO crystals with different in-planar doping and different oxygen chain structure were studied (see Table I). Except for the YBCO_{6.60} sample, detailed descriptions of these crystals are found in Refs. 12,26,27. The YBCO_{6.60} sample was studied with the scattering plane defined by $(k, k, 0)$ and $(0, 0, \ell)$. This configuration has the advantage that CDW modulations along both a - and b -axis directions could be accessed without reorienting the sample. The absence of $\ell = 0, 1$ CDW order along the a -axis direction was checked using the $(h, 0, \ell)$ scattering plane.

Data analysis h - and k -scans, as shown in Fig. 2(c,d), are fitted with a single Gaussian function on a weakly sloping background. ℓ -scans with a well-defined peak at $\ell = 1$ (1j and Fig. 2a-b) are fitted using a two Gaussian functions. Correlation lengths $\xi = 1/\sigma$ are defined by the inverse Gaussian standard deviation $\sigma = (\sigma_{\text{meas}}^2 - \sigma_R^2)^{0.5}$. The instrumental resolution σ_R – for a CDW reflection – was estimated at Bragg reflections near to the measured CDW reflections. Resolution corrected correlation lengths are given in table I.

Simulation of scattering profiles We use a simple Markov chain model²⁸ of order $m = 2$ to interpret the diffuse and $\ell = 1$ scattering profiles e.g. in Fig. 1j. A Markov chain is a stochastic series. Here we generate a series of two types of bilayer (A and B) corresponding to the phase of the displacement of the CDW in a given bilayer. We represent the bilayer type at position index i along the c -direction by a stochastic variable x_i . This can take either the value $x_i = 1$, denoting bilayer type A , or $x_i = 0$ for type B . We create a series of bilayers starting, for instance, with an A bilayer, followed by a B . The probability $P(x_i = 1)$ of adding an A bilayer at position i , preceded by x_{i-1} and x_{i-2} , in the series is given by:

$$P(x_i = 1 | x_{i-1}, x_{i-2}) = \alpha + \beta x_{i-1} + \gamma x_{i-2}. \quad (1)$$

Clearly, $P(x_i = 0) = 1 - P(x_i = 1)$. Eq. 1 is a recipe, using random numbers to represent the probabilities, to create a series of bilayers with a given amount of correlation built in. Let m_A ($m_B = 1 - m_A$) be the fraction of A -type (B -type) bilayers in the series and P_1^{AA} the proportion of AA bilayer pairs separated by one lattice spacing. We choose $\alpha = \frac{1}{2}(1 - \beta - \gamma)$ so that macroscopically $m_A = m_B = \frac{1}{2}$. A number ($N \sim 500$) of stochastic series x_i ($N_{\text{site}} = 100$) subject to a given α, β, γ are generated. The corresponding scattered intensity (assuming the single unit cell structure from Ref. 22) for each series is calculated and averaged. β, γ are adjusted to give the best fit to the data and P_1^{AA} is calculated.

- ¹ Fradkin, E., Kivelson, S. A. & Tranquada, J. M. Theory of intertwined orders in high temperature superconductors. *Rev. Mod. Phys.* **87**, 457–482 (2015).
- ² Efetov, K. B., Meier, H. & Pepin, C. Pseudogap state near a quantum critical point. *Nat. Phys.* **9**, 442–446 (2013).
- ³ Wu, T. *et al.* Magnetic-field-induced charge-stripe order in the high temperature superconductor $\text{YBa}_2\text{Cu}_3\text{O}_y$. *Nature* **477**, 191 (2011).
- ⁴ Grissonnache, G. *et al.* Onset field for Fermi surface reconstruction in the cuprate superconductor YBCO. arXiv:1508.05486.
- ⁵ LeBoeuf, D. *et al.* Thermodynamic phase diagram of static charge order in underdoped $\text{YBa}_2\text{Cu}_3\text{O}_y$. *Nat. Phys.* **9**, 79 (2012).
- ⁶ Gerber, S. *et al.* Three-dimensional charge density wave order in $\text{YBa}_2\text{Cu}_3\text{O}_{6.67}$ at high magnetic fields. *Science*, 5 November 2015 (10.1126/science.aac6257).
- ⁷ Maharaj, A. V. *et al.* Quantum oscillations in a bilayer with broken mirror symmetry: a minimal model for $\text{YBa}_2\text{Cu}_3\text{O}_{6+\delta}$. arXiv:1510.02116.
- ⁸ Briffa, A. *et al.* Fermi surface reconstruction and quantum oscillations in underdoped $\text{YBa}_2\text{Cu}_3\text{O}_{7-x}$ modeled in a single bilayer with mirror symmetry broken by charge density waves. arXiv:1510.02603.
- ⁹ Monceau, P. Electronic crystals: An experimental overview. *Adv. Phys.* **61**, 325–581 (2012).
- ¹⁰ Laliberté, F. *et al.* Fermi-surface reconstruction by stripe order in cuprate superconductors. *Nat. Comms.* **2**, 432 (2011).
- ¹¹ Ghiringhelli, G. *et al.* Long-range incommensurate charge fluctuations in $(\text{Y,Nd})\text{Ba}_2\text{Cu}_3\text{O}_{6+x}$. *Science* **337**, 821 (2012).
- ¹² Chang, J. *et al.* Direct observation of competition between superconductivity and charge density wave order in $\text{YBa}_2\text{Cu}_3\text{O}_{6.67}$. *Nat. Phys.* **8**, 871 (2012).
- ¹³ Achkar, A. J. *et al.* Distinct charge orders in the planes and chains of ortho-III ordered $\text{YBa}_2\text{Cu}_3\text{O}_{6+\delta}$ identified by resonant elastic x-ray scattering. *Phys. Rev. Lett.* **109**, 167001 (2012).
- ¹⁴ Comin, R. *et al.* Charge order driven by Fermi-arc instability in $\text{Bi}_2\text{Sr}_{2-x}\text{La}_x\text{CuO}_{6+\delta}$. *Science* **343**, 390–392 (2014).
- ¹⁵ da Silva Neto, E. H. *et al.* Ubiquitous interplay between charge ordering and high-temperature superconductivity in cuprates. *Science* **343**, 393–396 (2014).
- ¹⁶ Tabis, W. *et al.* Charge order and its connection with Fermi-liquid charge transport in a pristine high- T_c cuprate. *Nat. Comm.* **5**, 5875 (2014).
- ¹⁷ Chang, J. *et al.* Nernst and Seebeck coefficients of the cuprate superconductor $\text{YBa}_2\text{Cu}_3\text{O}_{6.67}$: A study of Fermi surface reconstruction. *Phys. Rev. Lett.* **104**, 057005 (2010).
- ¹⁸ LeBoeuf, D. *et al.* Electron pockets in the Fermi surface of hole-doped high- T_c superconductors. *Nature* **450**, 533 (2007).
- ¹⁹ Vignolle, B. *et al.* Coherent c -axis transport in the underdoped cuprate superconductor $\text{YBa}_2\text{Cu}_3\text{O}_y$. *Phys. Rev. B* **85**, 224524 (2012).
- ²⁰ Tranquada, J. M. *et al.* Evidence for stripe correlations of spins and holes in copper oxide superconductors. *Nature* **375**, 561 (1995).
- ²¹ Hücker, M. *et al.* Stripe order in superconducting $\text{La}_{2-x}\text{Ba}_x\text{CuO}_4$ for $0.095 \leq x \leq 0.155$. *Phys. Rev. B* **83**, 104506 (2011).
- ²² Forgan, E. M. *et al.* The nature of the charge density waves in under-doped $\text{YBa}_2\text{Cu}_3\text{O}_{6.54}$ revealed by x-ray measurements of the ionic displacements. arXiv:1504.01585.
- ²³ Moudden, A. H. *et al.* q_1 charge-density wave in NbSe_3 . *Phys. Rev. Lett.* **65**, 223–226 (1990).
- ²⁴ Wu, T. *et al.* Incipient charge order observed by NMR in the normal state of $\text{YBa}_2\text{Cu}_3\text{O}_y$. *Nat. Comms.* **6** (2015).
- ²⁵ Wu, T. *et al.* Emergence of charge order from the vortex state of a high temperature superconductor. *Nat. Comms.* **4**, 2113 (2013).
- ²⁶ Blackburn, E. *et al.* X-ray diffraction observations of a charge-density-wave order in superconducting ortho-II $\text{YBa}_2\text{Cu}_3\text{O}_{6.54}$ single crystals in zero magnetic field. *Phys. Rev. Lett.* **110**, 137004 (2013).
- ²⁷ Hücker, M. *et al.* Competing charge, spin, and superconducting orders in underdoped $\text{YBa}_2\text{Cu}_3\text{O}_y$. *Phys. Rev. B* **90**, 054514 (2014).
- ²⁸ Welberry, T. R. Diffuse x-ray scattering and models of disorder. *Rep. Prog. Phys.* **48**, 1543 (1985).
- ²⁹ Grissonnache, G. *et al.* Direct measurement of the upper critical field in a cuprate superconductor. *Nat. Comms.* **5**, 3280 (2014).

Acknowledgements:

We wish to thank M. H. Julien and L. Taillefer for helpful discussions. This work was supported by the EPSRC (grant numbers EP/G027161/1 and EP/J015423/1), the Danish Agency for Science, Technology and Innovation under DANSCATT and the Swiss National Science Foundation grant number BSSGI0-155873.

Author contributions:

R.L., D.A.B, W.H. grew and prepared the samples. J.C., E.B., M.H., N.B.C., U.R., M.Z., E.M.F., S.M.H. conceived and planned the experiments. J.C., E.B., O.I., A.H., M.Z., E.M.F., S.M.H. carried out the experiments. J.C., S.M.H. carried out the data analysis and modelling. All co-authors contributed to the manuscript.

Competing financial interest:

The authors declare no competing financial interests.

Additional information

Correspondence to: J. Chang (johan.chang@physik.uzh.ch) and S. M. Hayden (s.hayden@bristol.ac.uk).

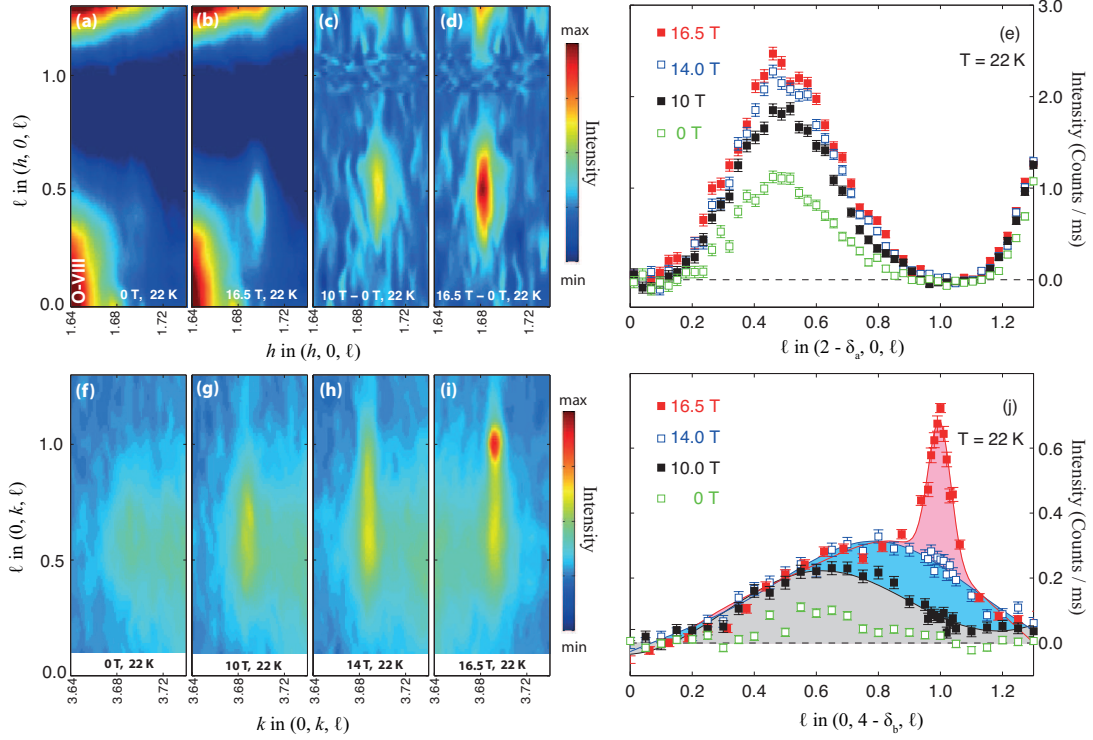


FIG. 1: **Charge-density-wave correlations induced by a magnetic field in $\text{YBa}_2\text{Cu}_3\text{O}_{6.67}$.** A magnetic field applied along the c -axis introduces new CDW correlations propagating along both CuO bond directions a and b in the CuO_2 planes. **a,b,f-i** Raw x-ray scattering intensity data for the $(h, 0, \ell)$ (top row) and $(0, k, \ell)$ (bottom row) planes for magnetic fields $0 \leq B \leq 16.5$ T. Strong features in **(a)** and **(b)** are due to CuO chain scattering. **c,d** Field induced scattering for $(h, 0, \ell)$. **e,j** CDW intensity along lines $\mathbf{Q} = n\mathbf{a}^* + m\mathbf{b}^* \pm \mathbf{q}_{a,b} + \ell\mathbf{c}^*$ isolated from data such as **(a,b,f-i)**. The CDW intensity has been isolated by fitting peaks due to the CDW and other structural features to a series of h - or k -cuts through data such as **(a,b,f-i)**. CDWs propagating along the a -axis (**a-e**) within individual bilayers become stronger without changing phase relationship with neighbouring bilayers. Those propagating along b -axis (**f-j**) become in-phase with neighbouring bilayers, which changes the profile in ℓ . The shaded areas in **(j)** show: weakly anticorrelated CDW (grey); 3D CDW precursor correlations (blue); 3D CDW order (red). Error bars are standard deviations determined by counting statistics. We describe reciprocal space as $\mathbf{Q} = h\mathbf{a}^* + k\mathbf{b}^* + \ell\mathbf{c}^*$, where $\mathbf{a}^* = 2\pi/a$, $a = 3.81$ Å, $b = 3.87$ Å and $c = 11.72$ Å.

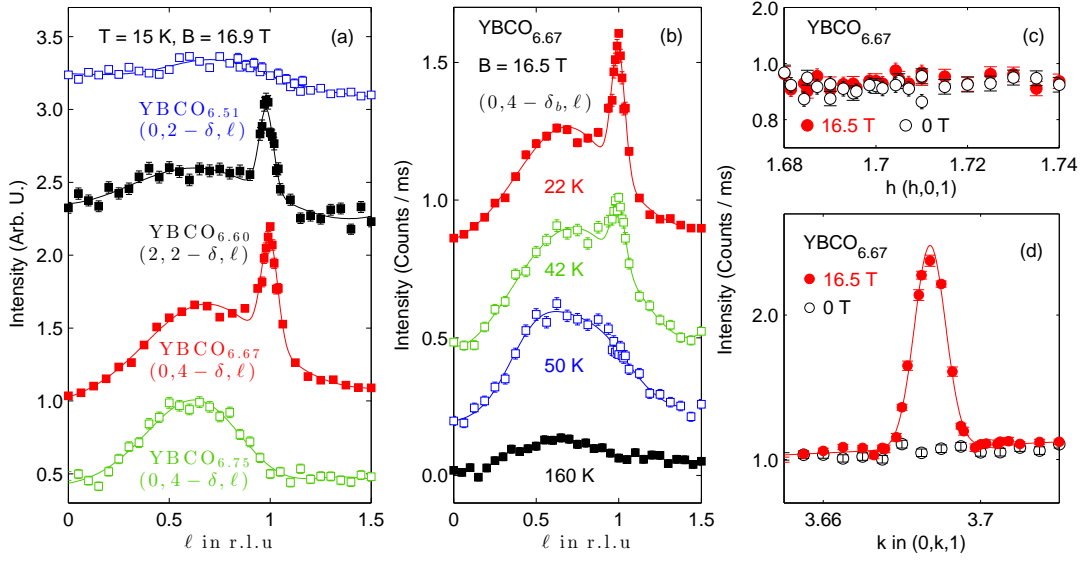


FIG. 2: **Doping, temperature and field dependence of induced CDW correlations.** **a** ℓ -scans along $(0, \delta_b, \ell)$ for different dopings of YBCO at $T \approx 8$ K and $B = 16.9$ T showing the field-induced 3D correlations or lack thereof. **b** Temperature dependence of ℓ -scans along $(0, \delta_b, \ell)$ measured on YBCO_{6.67} at $B = 16.5$ T. All curves in (a) and (b) have been given an arbitrary shift. **c,d** h -scans through $(2 - \delta_a, 0, 1)$ and k -scans through $(0, 4 - \delta_b, 1)$ in YBCO_{6.67} for zero-field and $B = 16.5$ T. Error bars are standard deviations determined by counting statistics.

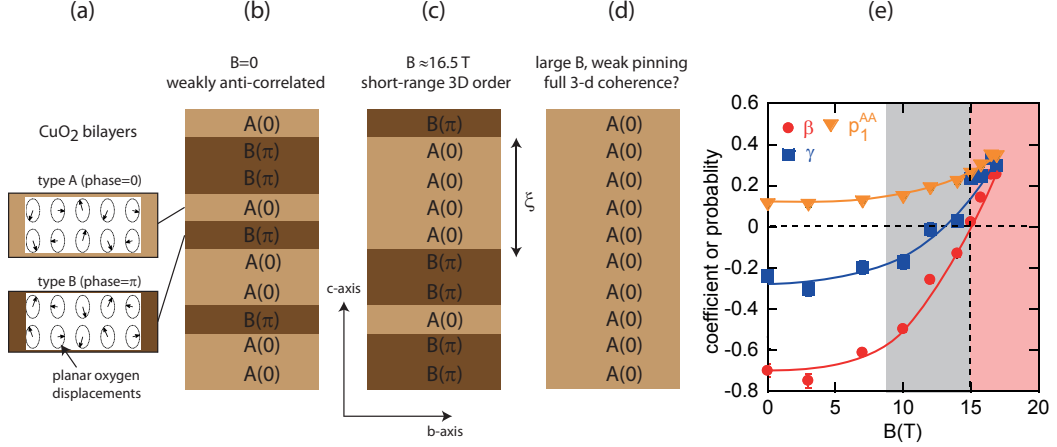


FIG. 3: **Magnetic field effect on c -axis correlations in YBa₂Cu₃O_{6+x}** **a** Schematic of the CDW modulation in a bilayer²². Arrows represent the displacement of the planar oxygens. Two phases: A ($\theta = 0$), B ($\theta = \pi$) of the modulation are shown. **b-d** Representative CDW stacking sequences for different fields. Increasing the field creates correlated regions of size $\xi_c \approx 4c$. **e** Field-dependent parameters determined from fitting data such as Fig. 1j to the Markov model described in Methods: nearest-neighbour coupling (β); next-nearest-neighbour coupling (γ); and the proportion of bilayer AA pairs separated by one lattice spacing (P_1^{AA}). Note $P_1^{BB} = P_1^{AA}$.

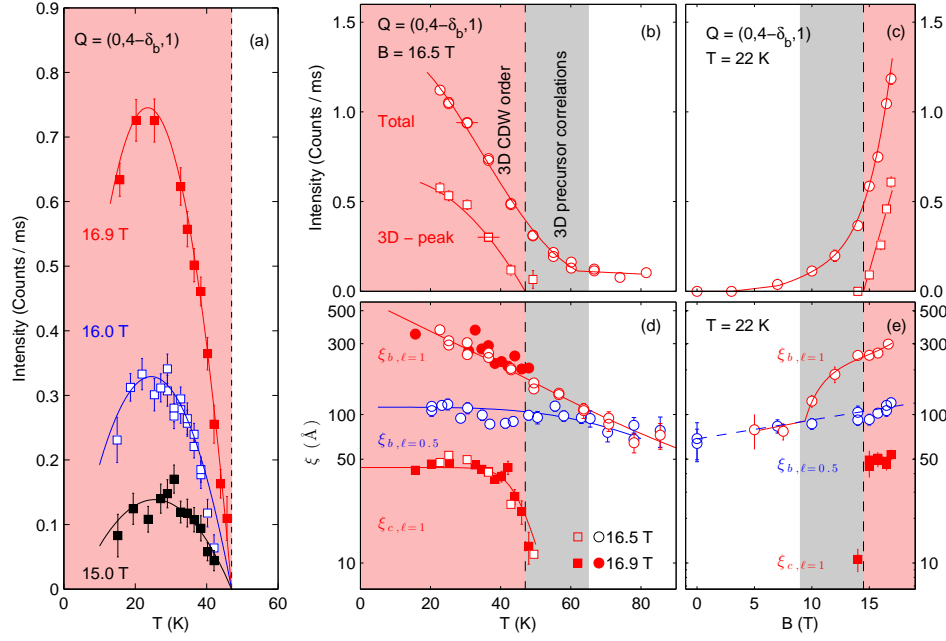


FIG. 4: **Evolution of charge-density-wave correlation lengths and intensities with magnetic field and temperature**
a Intensity of the 3D CDW peak extracted from ℓ -scans through $\mathbf{Q} = (0, 4 - \delta_b, \ell)$ versus temperature at fields as indicated.
b-c Total CDW intensity determined from k -scans (open circles) and 3D CDW peak intensity determined from ℓ -scans (closed squares) through the $(0, 4 - \delta_b, 1)$ position. **d,e** Correlation lengths $\xi_{b,\ell=1}$, $\xi_{c,\ell=1}$, $\xi_{b,\ell=1/2}$ determined from the resolution-corrected peak widths ($\sigma = \xi^{-1}$) of scans through $(0, 4 - \delta_b, 1)$, $(0, 4 - \delta_b, 1)$ and $(0, 4 - \delta_b, 1/2)$ positions respectively. Error bars are standard deviations of the fit parameters described in the Methods.

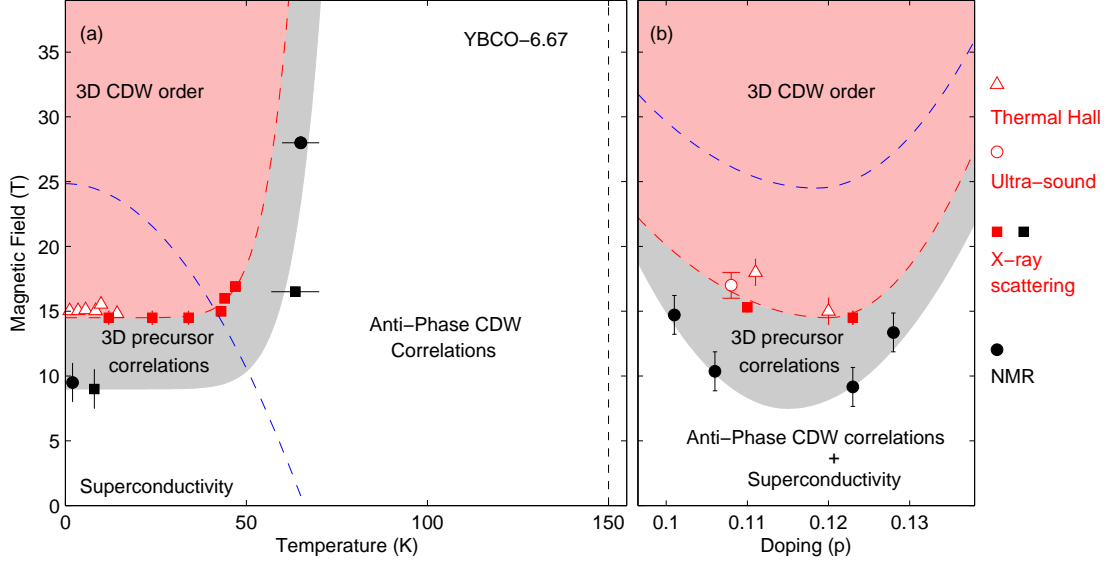


FIG. 5: **Phase diagram of $\text{YBa}_2\text{Cu}_3\text{O}_{6+x}$.** The pink shaded areas represent the regions where short range 3D CDW order exists. Grey bands indicate the regions where growing 3D CDW precursor correlations are observed. **a** Temperature-magnetic field phase diagram. **b** Doping-magnetic field phase diagram. Solid red square points indicate the onset of a 3D CDW order with $\mathbf{q}_b = (0, \delta_b, 0)$ determined from the variation of the $\xi_{c, \ell=1}$ correlation length and the intensity of the 3D peak (see Fig. 4). Triangles are the Fermi surface reconstruction onset determined from thermal Hall coefficient⁴. Solid black squares indicate the onset of growing in-plane CDW correlation lengths (3D precursor correlations) determined from the variation of $\xi_{b, \ell=1}$ (see Fig. 4d,e). Dashed blue lines in **(a)** and **(b)** indicate B_{c2} line²⁹. Solid black circles in **(a)** and **(b)** are derived from NMR^{3,25}. The vertical black dashed line is the onset of weakly anti-phase CDW correlations (Ref. 11–13). Red circular and triangular points originate from ultrasound⁵ and thermal Hall effect⁴ experiments whereas the red squares are the field onset of $\mathbf{q}_b = (0, \delta_b, 0)$ found by x-ray diffraction.